Size-Dependent Electrochemical Behavior of Thiol-Capped CdTe Nanocrystals in Aqueous Solution

Sergey K. Poznyak,[†] Nikolai P. Osipovich,[†] Alexey Shavel,[‡] Dmitri V. Talapin,[‡] Mingyuan Gao,[§] Alexander Eychmüller,[‡] and Nikolai Gaponik*,[‡]

Physico-Chemical Research Institute, Belarussian State University, 220050 Minsk, Belarus, Institute of Physical Chemistry, University of Hamburg, Grindelallee 117, D-20146 Hamburg, Germany, and Key Laboratory of Colloid, Interface Science and Chemical Thermodynamics, Institute of Chemistry, Chinese Academy of Science, Zhong Guan Cun, Bei Yi Jie 2, Beijing 100080, People's Republic of China

Received: August 31, 2004; In Final Form: October 19, 2004

Electrochemical studies of thiol-capped CdTe nanocrystals in aqueous solution have demonstrated several distinct oxidation and reduction peaks in the voltammograms, with the peak positions being dependent on the size of the nanocrystals. While the size dependence of the reduction and one of the oxidation potentials can be attributed to altering the energetic band positions owing to the quantum size effect, an extraordinary behavior was found for the oxidation peak observed at less positive potentials. In contrast to a prediction based on the quantum size effect, this peak moves to more negative potentials as the nanocrystals' size decreases. Moreover, the contribution of the charge associated with this peak compared to the total charge passed during the nanocrystal oxidation correlates well with the photoluminescence (PL) efficiency of individual fractions of the CdTe nanocrystals. These experimental observations allow a peak to be assigned to the oxidation of Te-related surface traps. The intra-band-gap energy level assigned to these Te-related trap states shifts toward the top of the valence band as the nanocrystal size increases, thus allowing the higher photostability of the larger nanocrystals to be explained. At a certain nanocrystal size, the trap level can even move out of the band gap.

1. Introduction

The unique size-dependent optical properties of colloidal semiconductor nanocrystals (NCs) have been the subject of considerable interest in the past two decades.[1,2] Strongly luminescing II−VI semiconductor NCs have found potential applications in biological imaging and labeling,[3−7] photovoltaics,[8] electroluminescence devices,[9−13] and so forth. Structural,[14] photophysical,[1,14−16] photochemical,[17,18] and photoelectrochemical[19−22] properties of the semiconductor NCs have been intensively studied; however, considerably less attention has been given to their electrochemical properties.[19,23−26] Several reports have been devoted to the study of a correlation between the optical band gap of the NCs and the band gap estimated from the oxidation and reduction peak positions in cyclic voltammograms.[24,25] These studies have been performed in nonaqueous media, and the results obtained are somewhat contradictory. Whereas Kucur et al.[25] found good agreement between electrochemical and optical E_g values for CdSe NCs with different sizes, Bard and co-workers[24] revealed that the electrochemical band gaps were smaller than the optical gaps for CdS NCs. In their recent work, Bard et al. found that the electrochemical band gap (∼2.1 eV) between the first anodic and cathodic peaks was close to the optical E_g value (2 eV) for TOPO-capped CdTe nanoparticles.[27] The authors of the electrochemical studies noted that upon changing the particle size the reduction and oxidation peaks in the voltammograms were shifted in the direction predicted by theory.[19,24,25,27]

Water soluble thiol-capped CdTe NCs have been demonstrated to be one of the most robust and highly fluorescent nanoparticle materials directly synthesized in an aqueous medium.[28] They can be successfully incorporated into ultrathin polymer films using the layer-by-layer assembly method.[11,29] Different color emissions can be electrically generated upon applying an external bias when the film is sandwiched between two conducting electrodes. Such electroluminescence devices have shown strong size-dependent electro-optical properties, such as electroluminescence efficiency and electrical conductivity.[11] In addition, the CdTe NCs also demonstrate a distinct size-dependent photostability.[28] Even taking into account the quantum size effect, it is still difficult to understand some of these size-dependent behaviors of the NCs. For nanoparticle materials, where the surface-to-volume ratio is considerably large, the state of the surface becomes important in determining many of the nanocrystal properties, for example, trapping of charge carriers and emission. Since the energy levels of surface traps are difficult to predict, a search for new approaches to their investigation is of current interest.

Here, we report the results of electrochemical studies on CdTe NCs with different sizes and (or) different optical properties by the use of cyclic voltammetry (CV). The motivation for this research was to investigate correlations between the electrochemical properties of CdTe NCs with different sizes and their optical properties and stability. The establishment of such correlations in aqueous buffer solutions is of special interest for bioapplications of NCs. Since the electrochemical degradation of nanoparticles should start from the particle surface, the CV method might also provide useful information on the surface of NCs.

2. Experimental Section

CdTe NCs stabilized by thioglycolic (TGA) or 3-mercaptopropionic (MPA) acids were synthesized according to the

* To whom correspondence should be addressed. E-mail: gaponik@chemie.uni-hamburg.de.
[†] Belarussian State University.
[‡] University of Hamburg.
[§] Chinese Academy of Science.

10.1021/jp0460801 CCC: $30.25
Published on Web 01/04/2005

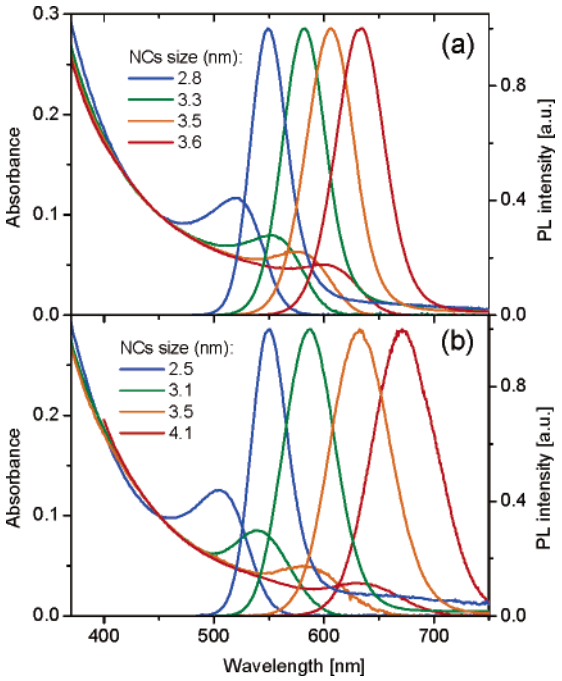

Figure 1. Absorption and PL spectra of TGA-capped (a) and MPA-capped (b) CdTe nanocrystals of four different sizes (λ_{ex} = 450 nm).

procedure described previously.[28] Briefly, $Cd(ClO_4)_2 \cdot 6H_2O$ was dissolved in water and TGA (or MPA) was added under stirring followed by adjusting the pH to 11.2−11.8 by dropwise addition of NaOH solution. H_2Te gas was passed through the solution together with nitrogen as a carrier gas. At this stage, CdTe precursors were formed. The precursors were converted to CdTe NCs by refluxing the reaction mixture at 100 °C. Portions of CdTe NCs of different sizes were taken from the crude solution at different refluxing times. Each portion of the crude solution was divided into a series of fractions with narrower size distributions by size-selective precipitation employing 2-propanol as a nonsolvent.[28] This procedure also allowed us to wash out the reaction byproducts and excessive stabilizing agents.

Figure 1 shows absorption and photoluminescence (PL) spectra of a number of TGA- and MPA-stabilized fractions of CdTe NCs which were chosen for the investigation of their size-dependent electrochemical properties. All colloids obtained possess a well-resolved absorption maximum of the first electronic transition indicating a sufficiently narrow size distribution of the NCs. The absorption maximum shifts to shorter wavelengths with decreasing NC size as a consequence of quantum confinement.

For electrochemical measurements, CdTe NC colloidal solutions (particle concentration in the range 2×10^{-6} to 4×10^{-6} M) in a buffer containing 0.1 M Na_2SO_4 and 0.02 M $Na_2B_4O_7$ (pH 9.2) were prepared. The CdTe NC colloids were sufficiently stable in the presence of this supporting electrolyte in the dark. After addition of the buffer solution, no noticeable changes of the colloids were found at least for periods of weeks as judged from their absorption and fluorescence spectra.

Electrochemical measurements were performed in a standard three-electrode two-compartment cell with a platinum counter electrode and an Ag|AgCl|KCl(sat.) electrode as the reference electrode (+0.201 V vs SHE). All potentials were determined with respect to this reference electrode and were controlled by a conventional potentiostat with a controller. The working electrode compartment of the electrochemical cell was separated from the counter electrode compartment by a fine porous glass membrane.

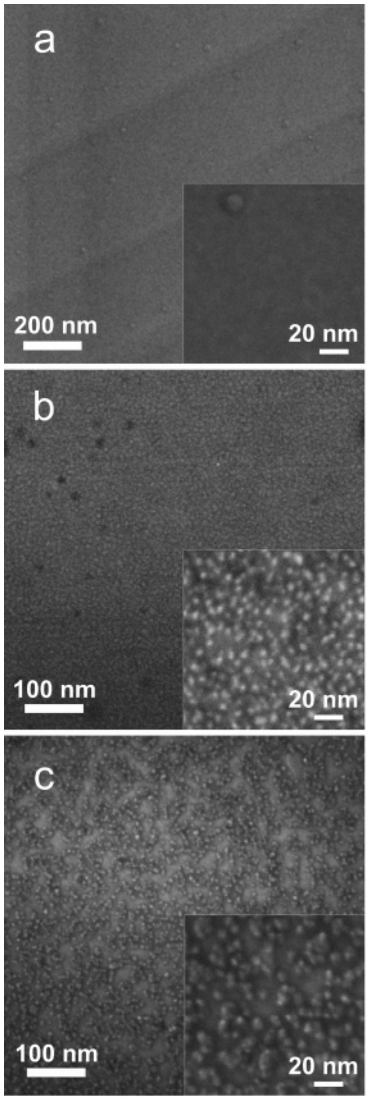

Figure 2. High-resolution SEM images of the surface of the Au electrode before (a) and after adsorption of CdTe nanocrystals stabilized with TGA (b) and MPA (c). The mean particle sizes as deduced from optical spectroscopy[36] were 3.3 and 7 nm for the TGA- and MPA-stabilized NCs, respectively.

Gold plates or indium tin oxide (ITO) films on a glass substrate were used as working electrodes. The surface of the gold plates was polished by diamond paste followed by treatment in boiling concentrated HNO_3 and H_2SO_4. Then, the gold electrodes were thoroughly washed with doubly distilled water and annealed at 700 °C for 15 min in air. ITO electrodes were cleaned with a mixture of aqueous solutions of NH_3 and H_2O_2 and rinsed thoroughly with doubly distilled water. Before the measurements, the electrodes were cycled in the supporting electrolyte in the potential region from −0.5 to 1.1 V.

A series of the electrochemical experiments was carried out using preadsorbed NCs. The cleaned electrodes were dipped into the deaerated colloidal solutions of the NCs for 5 min. This procedure results in the adsorption of NCs on the electrode surface (Figure 2). The nanocrystal-coated electrodes were then washed with buffer solution and transferred to the electrochemical cell under an argon atmosphere. The cell electrolyte was deaerated by purging purified argon for 30 min. Analytical-grade reagents and doubly distilled water were used for the electrolyte preparation.

The amount of CdTe adsorbed on the gold surface was determined by the following procedure. The gold substrate with

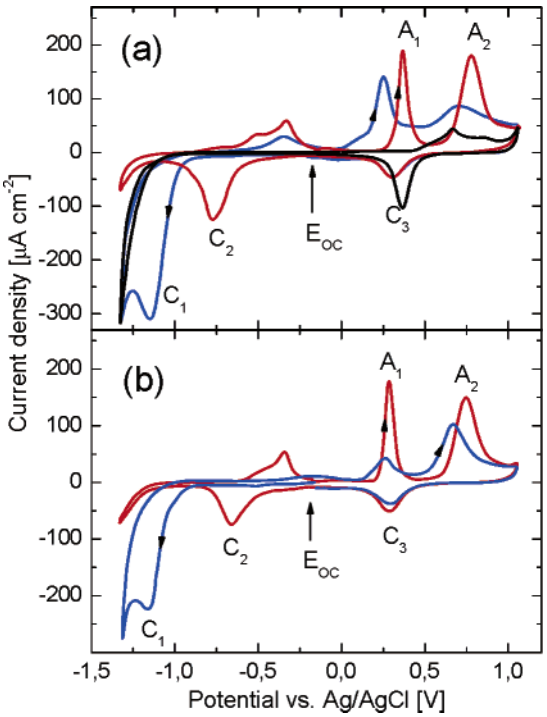

Figure 3. Voltammograms of the Au electrode in buffer solution containing TGA-capped CdTe nanocrystals (a) and Au electrodes with preadsorbed CdTe nanocrystals in blank buffer solution (b). The potential sweep direction was $-0.18 > 1.05 > -1.33 > -0.18$ V (red lines) and $-0.18 > -1.33 > 1.05 > -0.18$ V (blue lines). A cyclic voltammogram of the Au electrode in blank buffer solution is shown as a black line. The potential sweep rate was 20 mV s^{-1}. E_{OC}: open circuit potential.

the adsorbed NCs was rinsed with buffer solution and then treated in a definite portion of hot nitric acid. The concentration of Cd^{2+} ions in the resulting solution was determined by the use of an atomic emission spectrometer with an inductively coupled plasma excitation source (Spectroflame Modula). The roughness factor (f) of the Au electrodes was estimated according to the electrochemical method described previously.[30]

Ultraviolet−visible (UV−vis) absorption spectra were recorded with a Cary 50 spectrophotometer (Varian). Photoluminescence measurements were carried out at room temperature using a FluoroMax-2 spectrometer (Instruments SA).

High-resolution scanning electron microscopy (SEM) was done using a LEO 1550 microscope operating at 20 kV.

3. Results

3.1. Electrochemical Behavior of CdTe NCs on Au and ITO Electrodes. Figure 3a (black line) shows a cyclic voltammogram of the Au electrode in buffer solution. The current is negligible in the wide potential region from −1 to 0.5 V. Oxidation of the gold electrode surface starts from 0.5 V with an anodic current peak at 0.67 V that gives a cathodic current peak at 0.36 V (C_3) during the reverse potential scan.

Introducing the CdTe NCs into the buffer solution gives rise to a number of additional peaks on the CV curves of the Au electrodes (Figure 3a). When the potential is swept from the open circuit potential (E_{OC}) in the positive direction, two distinct anodic peaks can be recorded in the potential regions from 0.3 to 0.4 V (peak A_1) and from 0.75 to 0.8 V (peak A_2). The peak positions depend on the CdTe NC size (as will be shown below). At least two cathodic peaks (peak C_3 at 0.3 V, which is similar to the peak observed for the gold electrodes in blank buffer solution, and peak C_2 at −0.77 V) appear during the reverse potential scan. The subsequent potential cycling between −0.5 and 1.2 V results in the disappearance of peaks A_1 and A_2, and the CV curves become similar to those recorded in the supporting electrolyte, suggesting that the oxidation products block the electrode surface.

Figure 3a (blue line) also shows the first CV curve for the Au electrode in the CdTe NC colloidal solution by scanning the potential in the negative direction from the open circuit potential. A cathodic current peak, C_1, is observed at about −1.2 V, which is most likely associated with the reduction of the NCs. This peak is absent if the potential is initially scanned in the positive direction through peaks A_1 and A_2.

It should be noted that peaks A_1, A_2, and C_1 also occur in the voltammograms of the Au electrode in the case when the electrode after dipping into the CdTe NC colloidal solution is removed, rinsed with buffer solution, and immersed in a pure buffer electrolyte (Figure 3b). The open circuit potential of the Au electrode after its immersion in CdTe NC colloidal solution changes quickly in the negative direction and becomes stable after 1−2 min (Supporting Information Figure S1). These results indicate a strong and quick adsorption of CdTe NCs on the gold surface. The total charge of peaks A_1 and A_2 reaches a limiting value after ∼2 min of adsorption, providing additional support of this view. Characteristically, the charge corresponding to peaks A_1 and A_2 recorded in the buffer solution at the Au electrode with preadsorbed CdTe NCs and that recorded at the Au electrode immersed in CdTe NC colloidal solution coincide very well.

To obtain additional information on the redox reactions involving NCs, the dependence of the peak current and the potential on the scan rate were also studied (Supporting Information Figure S2). The positions of peaks A_1 and A_2 are shifted in the positive direction with increasing scan rate and the maximum current is linearly proportional to the scan rate, which is indicative of kinetic effects.

To elucidate if the substrate has an influence on the electrochemical behavior of the CdTe NCs, the same processes at ITO electrodes were studied. At the ITO electrode in blank buffer solution, the current is negligible in the potential region from −0.5 to 1.1 V (Supporting Information Figure S3). Upon addition of the CdTe NCs into the solution, an anodic wave starting at ∼0.2 V occurs. In the background of this wave, small peaks arise with potentials corresponding to those at the Au electrodes (Figure 3 and Supporting Information Figure S3). However, the charges corresponding to these peaks are significantly smaller than those recorded at the gold. One of the possible causes of this may be a weaker adsorption of NCs on the ITO surface.

3.2. Effect of Thiols on the Electrochemical Oxidation of CdTe Polycrystalline Thin Films and Nanocrystals. Thioglycolic or 3-mercaptopropionic acids were used as stabilizers for the CdTe NCs studied. Nevertheless, free thiols may be present even in redissolved and dialyzed solutions of CdTe NCs due to the adsorption equilibrium at the NC surface.[31] Stabilizer molecules in the NC colloidal solution also enhance the stability and influence luminescence properties.[28,31] Therefore, we studied the effect of thiols on the electrochemical oxidation of CdTe NCs.

Figure 4a shows the electrochemical behavior of TGA at the Au electrode in buffer solution. The open circuit potential of the immersed Au electrode is changed from 0.2 V (in buffer solution without TGA) to −0.45 V (in buffer solution containing 10^{-4} M TGA) due to the absorption of TGA on the gold surface. When scanning the potential in the positive direction, a wave

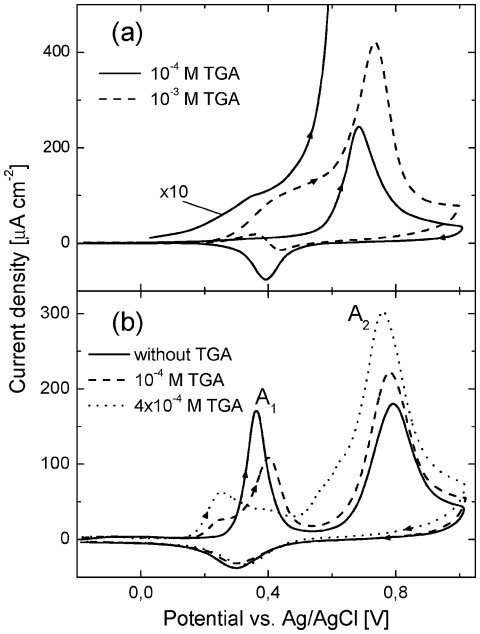

Figure 4. (a) Voltammograms of the Au electrodes in buffer solutions containing 10^{-4} and 10^{-3} M TGA. (b) Voltammograms of the Au electrode in CdTe nanocrystal colloidal solution (pH 9.2) without TGA and in that containing 10^{-4} M and 4×10^{-4} M TGA. The potential sweep rate was 20 mV s^{-1}.

at 0.4−0.5 V and an anodic peak at 0.68−0.75 V appear. The current in the region of 0.4−0.5 V is nearly proportional to the TGA concentration in solution. Similar CV curves were also obtained for the MPA solutions.

Figure 4b shows CV curves for the Au electrode in CdTe-NC-containing buffer solution with and without excess TGA. In the presence of 10^{-4} M TGA, peak A_1 is reduced and shifted in the positive direction. At the same time, a small new peak at ~0.25 V appears. With increasing TGA concentration, the peak at 0.25 V grows and peak A_1 decreases, being smaller in comparison to the former peak. Moreover, peak A_2 is shifted in the negative direction and its charge grows with increasing TGA concentration.

To gain a better understanding of the results obtained, the electrochemical behavior of polycrystalline CdTe thin films was also studied. The films were deposited on Au plates under potentiostatic polarization ($E = -0.3$ V) in a solution containing 1 M $Cd(NO_3)_2$, 10^{-3} M TeO_2, and 0.1 M HNO_3 ($T = 70$ °C) according to the method described previously.[32] This method allows one to obtain polycrystalline CdTe films of p-type conductivity. The CdTe film electrodes were rinsed with distilled water and studied immediately after their preparation.

As the potential is swept in the positive direction from the open circuit potential (~ −0.07 V), the oxidation of the CdTe thin film in buffer solution starts at ~0 V, resulting in an anodic current peak at 0.35−0.40 V (Figure 5). We performed a chemical analysis of the cell electrolyte after recording this peak and did not find any traces of cadmium or tellurium in solution. This fact indicates that this peak may be associated with the anodic passivation of the CdTe film surface. At $E > 0.65$ V, a sharp current rise related to the CdTe film stripping appears. Introducing 10^{-3} M TGA into the buffer solution results in the following changes of the behavior of the CdTe thin film electrode (Figure 5):

(i) The open circuit potential moves in the negative direction (~ −0.4 V).

(ii) The oxidation peak is markedly reduced and shifted in the positive direction.

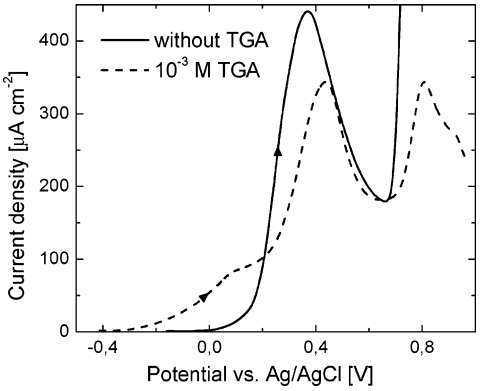

Figure 5. Anodic voltammograms of CdTe polycrystalline thin film electrodes in blank buffer solution and in buffer solution containing 10^{-3} M TGA. The potential sweep rate was 20 mV s^{-1}.

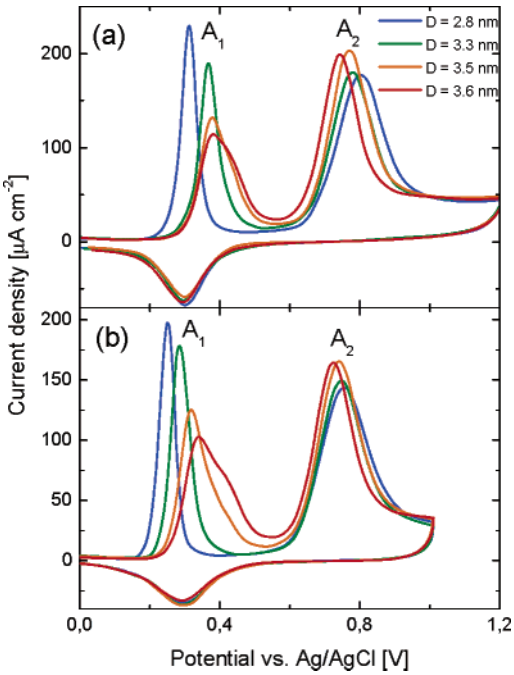

Figure 6. Voltammograms of the Au electrode in buffer solution containing TGA-capped CdTe nanocrystals of four different sizes (a) or in blank buffer solution after preadsorption of the same NCs on the Au electrode (b). The potential sweep rate was 20 mV s^{-1}.

(iii) An additional current shoulder at ~ −0.2 to 0.2 V appears.

(iv) The anodic current associated with the film dissolution at $E > 0.65$ V is significantly suppressed, indicating that TGA molecules promote the CdTe surface passivation.

This behavior is similar to that of CdTe colloidal NCs in the presence of excess TGA in solution (Figure 4b).

3.3. Size-Dependent Electrochemical Behavior of CdTe NCs. Figure 6 shows the first CV curves of the anodic dissolution of TGA-capped CdTe NCs of four different sizes at the Au electrode both in CdTe NC colloidal solution (a) and for preadsorbed NCs in the supporting electrolyte (b). Peak A_1 moves in the negative direction with decreasing NC size. At the same time, the position of peak A_2 depends less on the NC size than the position of peak A_1. It should be noted that, for the preadsorbed particles, the shift of peak A_1 is more pronounced and reproducible than in the case of colloidal solutions. Some amount of excess TGA in the NC colloids could be responsible for this difference, since, as shown above, thioglycolic acid influences markedly the A_1 peak position and

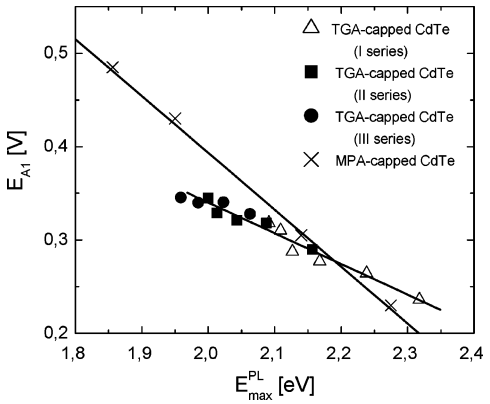

Figure 7. Dependence of the peak A_1 potential on the photon energy corresponding to the PL peak for three series of TGA-capped CdTe NC size-selected fractions and for a series of MPA-capped CdTe NC size-selected fractions.

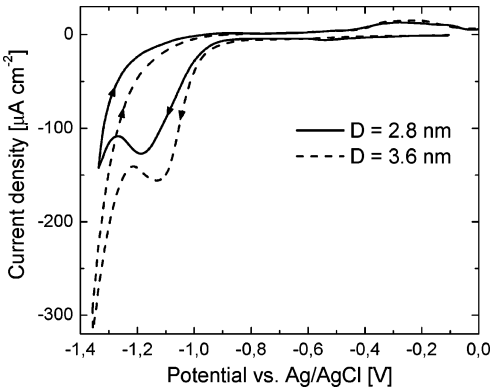

Figure 8. Cathodic voltammograms of the Au electrode in buffer solution after the preadsorption of TGA-capped CdTe nanocrystals of different sizes on the electrode surface. The potential sweep rate was 20 mV s^{-1}.

amplitude. Taking this fact into account, we carried out most of the measurements related to size-dependent effects at electrodes with preadsorbed NCs. A similar behavior was also revealed for the MPA-capped CdTe NCs (Supporting Information Figure S4).

Figure 7 presents the dependence of the potential corresponding to peak A_1 for the NCs of different sizes on the PL peak energy. To confirm reproducibility, three different size series of TGA-capped CdTe NCs were investigated. As can be seen, this dependence is practically linear both for TGA-capped and for MPA-capped CdTe NCs and the potential of the oxidation peak A_1 increases with increasing particle size or with decreasing NC band gap. Characteristically, the slope of the E_{A_1} versus $E^{PL}{}_{max}$ curve is markedly greater for MPA-capped NCs in comparison with TGA-capped ones.

Figure 8 depicts the first cyclic voltammograms of the cathodic reduction of TGA-capped CdTe NCs of two different sizes. The reduction peak C_1 also moves in the negative direction with decreasing NC size.

3.4. Correlation between PL Quantum Efficiencies and the Electrochemical Properties of CdTe NCs. It was shown recently that individual fractions of CdTe NCs separated from the same crude solution by size-selective precipitation could have different PL quantum yields. This difference exceeds an order of magnitude.[28,33,34] This phenomenon being typical for many types of colloidally synthesized NCs was investigated both theoretically[35] and experimentally,[33,34] and it was attributed to a dynamical distribution of growth conditions for the individual NCs in an ensemble growing by the Ostwald-ripening mechanism. Ostwald ripening is the growth mechanism in which smaller particles dissolve and the molecular species released thereby are consumed by the larger particles. Thus, in a colloidal solution of growing nanocrystals, the largest particles grow, the smallest dissolve, and the particles from the middle of the size distribution are in equilibrium with the surrounding solution. When the crude solution is taken from the reaction flask, both growth and dissolution are stopped due to the cooling. This crude solution of NCs can be divided into multiple fractions with narrower size distributions by size-selective precipitation. The NCs (and corresponding individual size-selected fractions) grown under conditions far away from the equilibrium of growth and dissolution have quite a low PL quantum yield and are named "lowly photoluminescent (LPL) fractions" in the following. Fractions grown under conditions close to the equilibrium have a high PL efficiency. These fractions are named "highly photoluminescent (HPL)" in the following. Moreover, by size selection from two different crude solutions grown under reflux for different amounts of time (5 h 40 min and 20 h in our case), it was possible to reach conditions where the HPL fraction separated from a longer refluxed solution was of the same size (i.e., of the same optical band gap) as the LPL fraction of a shorter refluxed one. The corresponding optical spectra are shown in Figure 9.

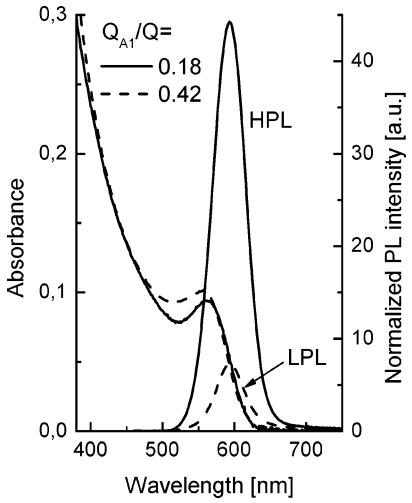

Figure 9. Absorption and PL spectra of high photoluminescent (HPL) and low photoluminescent (LPL) CdTe NC fractions of the same mean particles' size (see text for more details). The PL spectra are normalized to the absorption at the excitation wavelength (450 nm). The relative PL quantum yield for the HPL fraction is ~6 times higher than those of the LPL fraction (22 and 3.5%, respectively). The PL quantum yields were measured by comparison with an ethanol solution of rhodamine 6G.[28] The ratio between the relative charges associated with the oxidation peaks (A_1) is ~2.3.

In our present work, it was of interest to elucidate how the electrochemical properties of the individual selected fractions of CdTe NCs correlate with their optical properties. The charge of peak A_1 (Q_{A_1}) has been revealed to grow markedly by decreasing the PL quantum yield of NC colloids (both TGA and MPA stabilized) in a series of size-selected fractions and reach a maximum for the LPL fractions. We chose the Q_{A_1}/Q ratio (or relative charge associated with the A_1 oxidation peak) as a measure for this correlation. The total charge (Q) was calculated as $Q = (Q_{A_1} + Q_{A_2}) - Q_{C_3}$ to take into account the charge consumed by the gold surface oxidation which is close to the charge of the reduction peak C_3. As is seen from Figure 9, the ratio of the relative charges for the HPL and LPL fractions of the same mean particle size reaches ~2.3. Thus, the

TABLE 1: Comparison of the Band Gap Energies Estimated for TGA-Capped CdTe NCs of Three Different Sizes from the PL Maximum (E_g^{lum}) Position with the Electrochemical Estimates (ΔE) (the Difference between Oxidation and Reduction Peaks)

size of CdTe NCs,[a] nm	ΔE_1 (A_1-C_1),[b] V	ΔE_2 (A_2-C_1),[b] V	E_g^{lum}, eV
2.8	1.43	1.95	2.26
3.3	1.445	1.91	2.13
3.6	1.47	1.85	1.96

[a] The NC size was estimated using the energy of the first absorption peak.[36] [b] Peak separation at a scan rate of 20 mV s^{-1}.

phenomenon is purely attributed to the optical properties (PL quantum yield) and not to the NC size.

4. Discussion

In the present work, we have found that thiol-capped CdTe NCs can be adsorbed rapidly and firmly on a gold surface. This immobilization of the NCs occurs via thiol molecules used as stabilizing agents for the particles. AES analysis of sample solutions prepared by dissolving the adsorbed NCs with a 3.2 nm diameter (the particle size was estimated using the energy of the first absorption peak[36]) gave a surface concentration of $\sim 1.4 \times 10^{-9}$ mol of CdTe per 1 cm^2 of true surface area (taking into account the roughness factor of the gold electrode). The number of CdTe units in a 3.2 nm diameter NC, which was calculated from the volume ratio of the particle to the unit cell, is 253. Consequently, the adsorbed CdTe amount corresponds to $\sim 3.4 \times 10^{12}$ particles/cm^2. This surface concentration corresponds to $\sim$50% surface coverage, if we evaluate the thickness of the thiol-capping shell to be roughly 0.5 nm. This estimation is in good agreement with the results of SEM investigation of the surface of Au electrodes after adsorption of CdTe NCs (Figure 2). In contrast, the CdTe NCs are only weakly adsorbed on the ITO electrode surface.

The electrochemical studies revealed two rather well-defined anodic peaks, A_1 and A_2, in the positive potential region, which can be tentatively attributed to the anodic oxidation of CdTe NCs at the electrode surface according to the total reaction:

$$CdTe + 6OH^- \rightarrow Cd^{2+} + TeO_3^{2-} + 3H_2O + 6e^- \quad (1)$$

The total charge corresponding to peaks A_1 and A_2 is $\sim 980\ \mu C\ cm^{-2}$ for TGA-capped NCs with a 3.2 nm diameter. This value is in rather good agreement with the calculated value ($810\ \mu C\ cm^{-2}$) needed for the electrochemical oxidation of 1.4×10^{-9} mol of adsorbed CdTe according to reaction 1. Some discrepancy may be attributed to the fact that a part of the anodic charge can be consumed in the anodic oxidation of the thiol molecules from the NC shell. In the negative potential region, the electroreduction of the CdTe NCs is observed at potentials close to -1.2 V (Figures 3 and 8).

Since the positions of both the anodic and cathodic current peaks depend on the NC size, it was of interest to elucidate a relationship between electrochemical redox potentials and semiconductor band gap energies. The separation between peaks A_1 and C_1 is 1.4−1.6 V which is markedly smaller than the optical band gap of the CdTe NCs (2.0−2.3 eV) estimated from their spectra. At the same time, the A_2-C_1 peak separation correlates better with the optical gap, remaining slightly smaller than the latter value (Table 1).

According to our expectations, the smaller CdTe NCs should be oxidized at more positive potentials and reduced at more negative ones than the larger NCs, since the top of the valence band is shifted toward lower energies and the bottom of the conduction band is moved to higher energies with decreasing particle size. It is important to note that the direction of the size-dependent shift of peaks A_2 and C_1 is in accord with this expectation. In contrast, the oxidation peak A_1 behaves abnormally; that is, it shifts to the negative direction with decreasing NC size.

These observations allowed us to assume that peak A_1 can be related to the oxidation of surface defects forming intraband-gap surface states. The existence of trap states has been proven by fluorescence studies on CdS, CdSe, and CdTe NCs prepared in aqueous media.[14,37] Generally, the traps can be associated with both Cd and Te dangling bonds on the nanocrystal surface where the oxidation of CdTe NCs will start. Our previous high-resolution photoelectron spectroscopy study of TGA-capped CdTe NCs has revealed that a larger amount of surface Te atoms occurs on the surface of lowly luminescent NCs in comparison with highly luminescent ones.[33] The traps at the NC surface may give rise to nonradiative recombination pathways. Since the LPL samples possess much more Te atoms at the surface than the HPL ones, it becomes apparent why peak A_1, tentatively related to the oxidation of these traps, is markedly higher for the LPL fractions.

The shift of this peak to more positive potentials with increasing NC size indicates that the energy levels of Te-related traps move to lower energies when the NC size increases. Here, it is important to note that this effect is markedly dependent on the chain length of the thiol ligands. Figure 7 clearly demonstrates that peak A_1 is shifted more drastically to the positive direction with decreasing CdTe band gap for MPA-coated NCs as compared to TGA-coated ones. The shift becomes so large for the largest available NCs synthesized with MPA (PL maximum is $\sim$800 nm) that peak A_1 simply merges into peak A_2. This allows us to assume that for these NCs the energy levels of Te-related traps appear inside the valence band. For such a kind of particles, the highest possible photostability and PL lifetimes are expected, which corresponds very well with our preliminary observation.[38]

The above-mentioned trend can explain the higher photostability of the larger NCs. Moreover, it has previously been shown that photochemical etching results in both a significant improvement of the PL quantum yield and narrowing of the PL band of crude solutions of TGA-capped CdTe NCs owing to different rates of etching of different NCs in the ensemble.[28] This effect has been tentatively explained by the light-promoted oxidation of unsaturated Te atoms on the surface of high-defect NCs.

Along with the Te-related traps, TGA molecules adsorbed on the NC surface can be oxidized in the region of peak A_1. The appearance of the current shoulder at 0.25 V in the course of the NC oxidation in the presence of excess TGA in solution is probably due to the oxidation of TGA molecules diffusing to the surface of the CdTe NCs adsorbed on the Au electrode. Indeed, the TGA electro-oxidation proceeds with a lower overvoltage at the CdTe film in comparison with the Au electrode. The appearance of the shoulder is accompanied by a decrease in peak A_1. TGA molecules diffuse to the CdTe NCs anchored on the electrode surface, adsorb onto them, and are electrochemically oxidized, thus preventing the NCs from oxidation. The thiol ligands can convert into disulfides which can diffuse into the bulk solution without blocking the CdTe surface. This dynamic protection of the NCs can also explain the higher photostability of the CdTe NCs in the presence of an excess of free TGA in solution.[28,31,39]

Whereas the detailed mechanism of the electrochemical oxidation of the CdTe NCs remains largely unknown at the moment, the anodic peak A_2 is most likely to be due to the oxidation of the rest of the CdTe core. The adsorption of reaction products on the electrode surface (both at the Au and ITO electrodes) suppresses the nanocrystal electro-oxidation at the second and further scans. The electrochemical activity of thus passivated electrodes can be again restored by cleaning the electrode surface (see the Experimental Section). Since peak A_2 shifts only slightly in the positive direction with decreasing NC size, the electrochemical band gap calculated as an A_2-C_1 peak separation is less than the optical band gap especially for the smallest NCs. A similar difference has been previously observed for thioglycerol-capped CdS NCs and was attributed to a multielectron transfer process where the electrons (or holes) are consumed by fast coupled chemical reactions due to decomposition of the particles.[24] A total multielectron reaction usually involves several consecutive steps, and the redox potential of the rate-limiting step may be different from that of the total reaction. The irreversibility of the electrochemical oxidation of the CdTe NCs in aqueous solution (Figure 3) supports this assumption.

5. Conclusions

Electrochemical studies of thiol-capped CdTe NCs in an aqueous buffer solution (pH 9.2) have demonstrated several distinct oxidation and reduction peaks in the voltammograms, with the peak positions being NC size dependent. While the size dependence of the reduction (C_1) and oxidation (A_2) potentials can be attributed to moving the energetic band positions owing to the quantum size effect, an extraordinary behavior was found for the oxidation peak A_1 observed at less positive potentials. In contrast to our expectations, this peak moves to more negative potentials as the NC size decreases. Moreover, the contribution of the A_1 peak charge to the total charge passed during the NC oxidation correlates well with the PL efficiency of individual fractions of the CdTe NCs. These observations together with the literature data support an assignment of this peak to the oxidation of Te-related surface traps. The results obtained indicate that the energy levels of these traps are shifted to lower energies as the NC size increases, thus allowing the higher photostability of the larger NCs to be explained.

Thus, the current research has demonstrated that the CV method is very sensitive to the nanocrystal surface state, providing complimentary information for a better understanding of the special size-dependent optical properties of semiconductor NCs.

Acknowledgment. We thank Prof. Dr. Horst Weller, Dr. Stephen G. Hickey, and Dr. Andrey L. Rogach for useful discussions. We are deeply indebted to A. Kornowski for his assistance with the SEM. N.G. greatly acknowledges the possibility to perform a part of the experiments in the group and under the support of Prof. Dr. Jochen Feldmann (LMU Munich). This work was supported in part by the NATO Collaborative Linkage Grant PST.CGL.979631, the EU project "FUNLIGHT", and the DIP-project D3.1.

Supporting Information Available: Figures showing the evolution of the open circuit potential of the gold electrode in contact with the CdTe NC solution, the dependence of CV peak positions on the potential scan rate, the CV plots of CdTe NCs on ITO electrodes, and the size-dependent electrochemical properties of MPA-stabilized CdTe NCs. This material is available free of charge via the Internet at http://pubs.acs.org.

References and Notes

(1) Gaponenko, S. V. *Optical Properties of Semiconductor Nanocrystals*; Cambridge University Press: Cambridge, U.K., 1998.
(2) Alivisatos, A. P. *J. Phys. Chem.* **1996**, *100*, 13226.
(3) Kim, S.; Bawendi, M. G. *J. Am. Chem. Soc.* **2003**, *125*, 14652.
(4) Dubertret, B.; Skourides, P.; Norris, D. J.; Noireaux, V.; Brivanlou, A. H.; Libchaber, A. *Science* **2002**, *298*, 1759.
(5) Alivisatos A. P. *Nat. Biotechnol.* **2004**, *22*, 47.
(6) Jaiswal, J. K.; Mattoussi, H.; Mauro, J. M.; Simon, S. M. *Nat. Biotechnol.* **2003**, *21*, 47.
(7) Han, M.; Gao, X.; Su, J. Z.; Nie, S. *Nat. Biotechnol.* **2001**, *19*, 631.
(8) Huynh, W. U.; Dittmer, J. J.; Alivisatos, A. P. *Science* **2002**, *295*, 2425.
(9) Schlamp, M. C.; Peng, X.; Alivisatos, A. P. *J. Appl. Phys.* **1997**, *82*, 5837.
(10) Mattoussi, H.; Radzilowski, L. H.; Dabbousi, B. O.; Thomas, E. L.; Bawendi, M. G.; Rubner, M. F. *J. Appl. Phys.* **1998**, *83*, 7965.
(11) Gao, M.; Lesser, C.; Kirstein, S.; Möhwald, H.; Rogach, A. L.; Weller, H. *J. Appl. Phys.* **2000**, *87*, 2297.
(12) Steckel, J. S.; Coe-Sullivan, S.; Bulovic, V.; Bawendi, M. G. *Adv. Mater.* **2003**, *15*, 1862.
(13) Koktysh, D. S.; Gaponik, N.; Reufer, M.; Crewett, J.; Scherf, U.; Eychmüller, A.; Lupton, J. M.; Rogach, A. L.; Feldmann, J. *ChemPhysChem* **2004**, *5*, 1435.
(14) Eychmüller, A. *J. Phys. Chem. B* **2000**, *104*, 6514.
(15) Sharma, S. N.; Pillai, Z. S.; Kamat, P. V. *J. Phys. Chem. B* **2003**, *107*, 10088.
(16) Lifshitz, E.; Glozman, A.; Litvin, I. D.; Porteanu, H. *J. Phys. Chem. B* **2000**, *104*, 10449.
(17) Jones, M.; Nedeljkovic, J.; Ellingson, R. J.; Nozik, A. J.; Rumbles, G. *J. Phys. Chem. B* **2003**, *107*, 11346.
(18) Aldana, J.; Wang, Y. A.; Peng, X. *J. Am. Chem. Soc.* **2001**, *123*, 8844.
(19) Ogawa, S.; Hu, K.; Fan, F.-R. F.; Bard, A. J. *J. Phys. Chem. B* **1997**, *101*, 5707.
(20) Talapin, D. V.; Poznyak, S. K.; Gaponik, N. P.; Rogach, A. L.; Eychmüller, A. *Physica E* **2002**, *14*, 237.
(21) Hickey, S. G.; Riley, D. J.; Tull, E. J. *J. Phys. Chem. B* **2000**, *104*, 7623.
(22) Torimoto, T.; Tsumura, N.; Nakamura, H.; Kuwabata, S.; Sakata, T.; Mori, H.; Yoneyama, H. *Electrochim. Acta* **2000**, *45*, 3269.
(23) Chen, S.; Truax, L. A.; Sommers, J. M. *Chem. Mater.* **2000**, *12*, 3864.
(24) Haram, S. K.; Quinn, B. M.; Bard, A. J. *J. Am. Chem. Soc.* **2001**, *123*, 8860.
(25) Kucur, E.; Riegler, J.; Urban, G. A.; Nann, T. *J. Chem. Phys.* **2003**, *119*, 2333.
(26) Ding, Z.; Quinn, B. M.; Haram, S. K.; Pell, L. E.; Korgel, B. A.; Bard, A. J. *Science* **2002**, *296*, 1293.
(27) Bae, Y.; Myung, N.; Bard, A. J. *Nano Lett.* **2004**, *4*, 1153.
(28) Gaponik, N.; Talapin, D. V.; Rogach, A. L.; Hoppe, K.; Shevchenko, E. V.; Kornowski, A.; Eychmüller, A.; Weller, H. *J. Phys. Chem. B* **2002**, *106*, 7177.
(29) Gao, M.; Sun, J.; Dulkeith, E.; Gaponik, N.; Lemmer, U.; Feldmann, J. *Langmuir* **2002**, *18*, 4098.
(30) Brummer, S. B.; Makrides, A. C. *J. Electrochem. Soc.* **1964**, *111*, 1122.
(31) Döllefeld, H.; Hoppe, K.; Kolny, J.; Schilling, K.; Weller, H.; Eychmüller, A. *Phys. Chem. Chem. Phys.* **2002**, *4*, 4747.
(32) Panicker, M. P. R.; Knaster, M.; Kroger, F. A. *J. Electrochem. Soc.* **1978**, *125*, 566.
(33) Borchert, H.; Talapin, D. V.; Gaponik, N.; McGinley, C.; Adam, S.; Lobo, A.; Möller, T.; Weller, H. *J. Phys. Chem. B* **2003**, *107*, 9662.
(34) Talapin, D. V.; Rogach, A. L.; Shevchenko, E. V.; Kornowski, A.; Haase, M.; Weller, H. *J. Am. Chem. Soc.* **2002**, *124*, 5782.
(35) Talapin, D. V.; Rogach, A. L.; Haase, M.; Weller, H. *J. Phys. Chem. B* **2001**, *105*, 12278.
(36) Yu, W. W.; Qu, L.; Guo, W.; Peng, X. *Chem. Mater.* **2003**, *15*, 2854.
(37) Weller, H.; Eychmüller, A. *Advances in Photochemistry*; Neckers, D. C., Volman, D. H., Bünau, G. v., Eds.; John Wiley & Sons: New York, 1995; Vol. 20, p 165.
(38) Franzl, T.; Shavel, A.; Gaponik, N.; Rogach, A. L.; Feldmann, J.; Eychmüller, A. Manuscript in preparation.
(39) Gao, M.; Kirstein, S.; Möhwald, H.; Rogach, A. L.; Kornowski, A.; Eychmüller, A.; Weller, H. *J. Phys. Chem. B* **1998**, *102*, 8360.